Evidence for strain control of magnetic anisotropy in epitaxial nickel ferrite thin films grown on strontium titanate substrates

Ying Liu,^{1,2} Zhiheng Mei,¹ Yizhong Guo,¹ Peng Zhou,¹ Yajun Qi,^{1,3*} Kun Liang,¹ Zhijun Ma,¹ Zhengcai Xia,⁴ Amitava Adhikary⁵, Cunzheng Dong⁶, NianXiang Sun,⁶ Gopalan Srinivasan², and Tianjin Zhang^{1*}

¹Hubei Collaborative Innovation Center for Advanced Organic Chemical Materials, Key Laboratory of Green Preparation and Application for Materials, Ministry of Education, Hubei Provincial Key Laboratory of Polymers, Department of Materials Science and Engineering, Hubei University, Wuhan 430062, China

This report is on strain control of magnetic order parameters in 50 nm epitaxial NiFe₂O₄ (NFO) films grown on (001), (110), and (111) SrTiO₃ (STO) single-crystal substrates by pulsed laser deposition. The related in-plane strains for NFO films on (001), (110), and (111) STO substrates are found to be -1.36%, 1.35%, and 1.52%, respectively, where the lattice mismatch between film and substrate is as high as 6.7%. Our analysis of magnetization and ferromagnetic resonance on all the NFO films reveals the presence of a uniaxial anisotropy field, which is perpendicular to the film plane. The anisotropy field decreases with the increase of strain in NFO films. Specifically, NFO films on STO (111) and STO (001) have the lowest and highest uniaxial anisotropy fileds of 1.4 kOe and 6.1 kOe, respectively. These experimental values of anisotropy field are a factor of 5 to 10 times smaller than those of the calculated ones due to the film defects induced by the high lattice mismatch. The studies of magnetic anisotropy of spinel ferrite films are of interest for spintronics and microwave devices.

Authors to whom correspondence should be addressed; email: <u>yjqi@hubu.edu.cn</u> (Y. J. Qi), <u>zhangtj@hubu.edu.cn</u> (T. J. Zhang)

²Physics Department, Oakland University, Rochester, Michigan 48309, USA

³Hubei Key Laboratory of Ferro & Piezoelectric Materials and Devices, Faculty of Physics & Electronic Science, Hubei University, Wuhan, 430062, China

⁴Wuhan National High Magnetic Field Center, Huazhong University of Science and Technology, Wuhan 430071, China

⁵Department of Chemistry, Oakland University, Rochester, Michigan 48309, USA

⁶Department of Electrical & Computer Engineering, Northeastern University, Boston, Massachusetts, 02115, USA

1. Introduction

Spinel ferrites attract extensively attentions with their unique magnetic order parameters, and show promising applications in spintronics, magnetoelectric sensors, and microwave devices. The study of magnetic order parameters in thin films of spinel ferrites induced by strain engineering has been of particularly attractive among the variety of controlling approaches. Recently, strain shows potential in inducing a large magnetic anisotropy in spinel ferrites, the understanding and enhancement of magnetic anisotropy has salient impact for the development and utilization of magnetic devices. To

Nickel ferrite (NiFe₂O₄, NFO), has an inverse spinel structure, with the two ferromagnetic order ions Fe3+ and Ni2+ occupied the tetragonal A sites and octahedral B sites of the spinel structure, respectively, shows high magnetic moment and low damping at room temperature. Recently, the study on magnetic property of NFO thin film in spintronics attracts lots of interests, such as the observation of spin seebeck effect in NFO films attributed to the magnetic anisotropy, 10 the tuning of spin hall magnetoresistance in NFO films by interface effect, 11 and the angle dependent of spin seebeck effect in NFO films provides a new way to investigate the magnetic anisotropy.¹² Furthermore, the strain control of magnetic anisotropy also have a significant contribution to the magnetic energy as a result of the large magnetostriction of NFO.¹³ Several reports have emphasized the importance of the strain effects on the anisotropic properties of pure and substituted NFO thin films. 14, 15 Recent reports in this regard include film-substrate lattice mismatch induced anisotropy field H_u as high as 10 kOe for films of NiZnAl-ferrite on (001) MgAl₂O₄ substrates¹⁶ and H_u ranging from 0.5 to 11.9 kOe for NFO films on (001) MgAl₂O₄, MgGa₂O₄, and CoGa₂O₄. ¹⁷ Some studies reported a giant saturation magnetization $M_{\rm s} \approx 771~{\rm emu/cm^3}$ for 2.6 nm NFO film on (001) SrTiO_{3.} ¹⁸ and the cause of such variations in the magnetization was attributed to the growth mechanisms and antiphase domains boundary in films.^{6,19} Most studies of magnetic anisotropy in epitaxial NFO thin film are focused mainly on films with a

particular crystallographic orientation, and there is a lack of study aimed at an understanding of the magnetic anisotropy as a function of substrate/film orientation for NFO thin films.

In this work, we report strain control of magnetic anisotropy for epitaxial NFO thin films fabricated on (001)-, (110)-, and (111)-oriented SrTiO₃ (STO) single crystal substrates. The choosing of STO substrate is due to the large lattice mismatch of 6.7% between STO and NFO. We are able to estimate both the magnetization and the growth induced uniaxial anisotropy H_u from the magnetization and FMR measurements. We inferred from these measurements that a large out-of-plane uniaxial anisotropy field H_u is present with the smallest value of $H_u = 1.4$ kOe for NFO/STO (111) and the highest value of 6.1 kOe for NFO/STO (001). The anisotropy fields H_u were compared with estimated values H_{σ} based on strain in the films and magnetostriction measured on a bulk NFO single crystal. Our results are of importance for the control of the growth induced anisotropy field in thin ferrite films for possible use in spintronic as well as microwave devices.

2. Experiment

NFO epitaxial thin films were deposited on (001)-, (110)- and (111)-oriented STO substrates by pulsed laser deposition.²⁰ The fabrication was carried out at 700 °C under an oxygen partial pressure of 15 Pa, the distance between target and substrate is 60 mm. The three oriented NFO thin films were simultaneously deposited on 0.5 mm thick 3×3 mm² STO substrates with a laser energy of 300 mJ at repetition rate of 5 Hz. After the fabrication, all the samples were annealed in air at 800 °C for 4 hrs.

The structural properties were measured by high-resolution X-ray diffraction (XRD) using a Bruker D8 Discover four-circle diffraction system (Cu $K_{\alpha 1}$, $\lambda = 1.5406$ Å) and a transmission electron microscope (TEM, Tecnai G20). Reciprocal Space Mappings (RSMs) were measured by high-resolution XRD using a PANalytical Empyrean four-circle diffraction system (Cu $K_{\alpha 1}$, $\lambda = 1.5406$ Å) with hybrid

monochromator and PIXcel3D detector. Magnetic properties were examined using a Superconducting Quantum Interference Device (SQUID-Quantum Design). Magnetization was measured for static magnetic field H either parallel or perpendicular to the film plane. A Varian Century Series X-band (9.3 GHz) ESR spectrometer with an E-4531 dual cavity, 9-inch magnet, and a 200 mW Klystron is used for FMR measurement. We employed the single cavity option, a TE_{102} -reflection type cavity with Q ~ 1000 was used. All ESR/FMR spectra were recorded at room temperature and at very low microwave power (6.3 μ W) to avoid sample heating.

3. Results and discussion

The XRD θ -2 θ patterns of NFO thin films **grown on (001)-, (110)-, and** (111)-oriented STO substrates are shown in Figure 1. Only the (00L), (LL0), and (LLL) diffraction peaks of NFO films can be detected, indicating the purity phase and epitaxial growth of NFO films. The epitaxial relationship between NFO thin films and STO substrates can be revealed by RSM, as shown in Figure 2. The RSMs were collected around the (004), (440), and (444) crystallographic planes for (001)-, (110)-and (111)-oriented films, respectively, and the NFO diffraction spots were lined up with STO spots along Q_y axis. The broadened RSM peaks for NFO films along Q_x direction indicate the presence of mosaic domain structure, and the peak of (111) STO substrate shows multiple diffraction spots, which could result in microstructural defects in NFO thin film. 21,22

Figure 3 shows the TEM cross-sectional images and selected area electron diffraction (SAED) patterns for (001)-, (110)-, and (111)-oriented NFO thin film. The thickness of the film was determined to be ~50 nm. The SAED and high resolution TEM results reveal that the NFO films was epitaxially grown on the three oriented STO substrates. The orientation relations between the thin film and the substrate are (001)NFO//(001)STO and [010]NFO//[010]STO, NFO(110)||STO(110) and NFO[110]||STO[110], (111)NFO//(111)STO and [121]NFO//[121]STO which are in agreement with the results of the RSMs. There is no separation of the spots

in diffraction patterns indicating the NFO films are under the strain states.

The lattice constants for NFO and the STO substrate are 8.339 Å and 3.905 Å, respectively. The lattice mismatch defined as $|a_{NFO}-a_{STO}|/a_{STO}$, where a_{NFO} is the bulk lattice constant of NFO and a_{STO} is the lattice constant of STO substrate in the direction relevant for the strain. So, the lattice mismatch between NFO film and STO substrate is 6.7%, calculated for two-unit cells of STO. From the XRD and RSM results, the out-of-plane lattice parameters for the three oriented-NFO films can be obtained using the Bragg equation, then the interplanar distances for (001), (110), and (111) orientations can be calculated. Both the NFO bulk and thin film values are discussed later. The atomic force microscopy topography of all the NFO films display a smooth surface, which is not shown here but the root mean square roughness is less 2 nm at area of $5 \times 5 \mu m^2$ for the films.

Figure 4 shows the measured magnetization as a function of H for the films. Normalized magnetization M/M_s vs H for the three films for H either parallel or perpendicular to the film plane are shown for H-values up to 20 kOe at room temperature. The applied field is along [100], [001], and [110] direction for (001)-, (110)-, and (111)-oriented NFO films. The diamagnetic contributions from STO substrates with different crystallographic orientation were subtracted. The saturation magnetization $M_s = 241$ emu/cc for (001)- and (111)-oriented NFO films, and 200 emu/cc for (110)-oriented NFO film, which are smaller than its bulk value. The S-shape in-plane and out-of-plane magnetic hysteresis loops are almost overlapped for all three oriented NFO films, the large coercive field and saturation magnetic field of all the NFO films indicate the defect of antiphase boundaries in films. The shape in-plane in films. The indicate the defect of antiphase boundaries in films.

In order to further investigate the nature of growth induced magnetic anisotropy in the NFO films in detail, in-plane and out-of-plane FMR measurements were carried out at **microwave frequency of** 9.3 GHz. For in-plane resonance, the applied magnetic field H was parallel to (111) plane of NFO for the film on **STO** (111), and along the [100] and [001] direction of NFO films on (001) and (110) substrates of STO, respectively. For H perpendicular to the sample plane, H was applied parallel to

[001], [110], or [111] direction of NFO films, respectively. The FMR profiles of the first derivative of power absorbed vs H are shown in Fig.5. The profiles show resonance with the line-width ΔH ranging from a minimum of 806 Oe to a maximum of 1225 Oe for in-plane fields. For out-of-plane static field, ΔH varies in the range of 580 Oe \sim 1370 Oe. The linewidth for NFO films on STO is much high than NFO films on MgGa₂O₄ and CoGa₂O₄,²⁵ that can be attributed to the large film-substrate mismatch of NFO and STO substrate. The larger mismatch could increase the density of antiphase domain boundaries in the film and thus resulting in the broad FMR pofiles,^{6,17-19} The presence of mosaics domain in NFO thin films observed in the RSM results in Fig. 2 could also contribute to broadening of FMR.

The resonance condition for in-plane FMR and the condition for equilibrium relating the orientations of magnetization and applied fields are given by ^{22,26,27}:

$$\left(\frac{f_{\rm r}}{\gamma}\right)^2 = \left[H_{\parallel} \cdot \cos(\Psi_{\rm M} - \Psi_{\rm H}) + 4\pi M_{\rm eff} + \frac{H_4}{4} \cdot (3 + \cos 4\Psi_{\rm M})\right] \cdot \left[H_{\parallel} \cdot \cos(\Psi_{\rm M} - \Psi_{\rm H}) - (4\pi M_{\rm S} - 4\pi M_{\rm eff}) \cdot \cos 2(\Psi_{\rm M} - \delta) + H_4 \cdot \cos 4\Psi_{\rm M}\right]$$
(1)

$$H_{\parallel} \cdot \cos(\Psi_M - \Psi_H) + \frac{H_4}{4} \cdot \sin 4\Psi_M = 0 \tag{2}$$

where ψ_M and ψ_H describe the orientation of applied field H and magnetization vector M, respectively, as shown in the inset of Fig. 5(a), $\delta = 45^{\circ}$, f_r is the resonance frequency, H_{\parallel} is the in-plane resonance field, and H_4 is the cubic magnetocrystalline anisotropy field. In Eqs. (1) and (2), $4\pi M_s$ is the saturation magnetization, $4\pi M_{\text{eff}}$ is the effective magnetization, γ is the gyromagnetic ratio for NFO which is assumed to be 3 GHz/kOe²⁵. The resonance condition is the same for H along [100] for NFO/STO (001) and along [001] for NFO/STO (110). Since (111) plane is magnetically isotropic, the same resonance condition could be used for H parallel to the plane of NFO/STO (111) assuming the same contribution from H_4 in all the three cases. The resonance fields are obtained from the FMR data and the saturation magnetization $4\pi M_s$ can be obtained from M vs H data in Fig. 4. The value of H_4 in single crystals of NFO is -500 Oe, 28 whereas $H_4 = -78$ Oe to -320 Oe for NFO films on substrates such as MgAl₂O₄ and MgGa₂O₄¹. Here, we assume $H_4 = -0.5$ kOe for NFO films and ψ_H is 0° for in-plane FMR, so that ψ_M can be estimated using Eq. (2)

and then $4\pi M_{\text{eff}}$ can be calculated from Eq. (1). Calculated values of ψ_M and $4\pi M_{\text{eff}}$ from in-plane FMR data are given in Table 1.

The growth induced uniaxial anisotropic field H_u is defined by $4\pi M_{\rm eff} = 4\pi M_{\rm s} - H_u$ and the calculated values H_u for (001), (110) and (111)-oriented NFO films are 6.128, 5.823 and 1.463 kOe, respectively. All the NFO thin films have the growth-induced out-of-plane anisotropy field H_u with the (111)-oriented NFO film having the lowest H_u and (001)-oriented film has the highest H_u . A similar determination of equilibrium orientation for magnetization θ and anisotropy fields could be determined from the resonance and equilibrium conditions for H perpendicular to the sample plane.²² Estimated values of θ from the equilibrium condition and magnetic parameters are given in Table 1.

For comparison with H_u , we estimated the strain anisotropy $H_{\sigma} = 3\lambda\sigma/M_s$ using the bulk magnetostriction values, the stress σ and saturation magnetization M_s of thin films.^{17,29} Figure 6 shows the magnetostriction we measured for a disk of NFO (110) single crystal. A strain gage and a strain indicator were used for measurements of λ with H along the 3 principal directions [001], [1, $\bar{1}$,0] and [1, $\bar{1}$,1]. The magnetostriction values are $\lambda_{001} = 40$ ppm, $\lambda_1 \bar{1}_0 = 18$ ppm, and $\lambda_1 \bar{1}_1 = 15$ ppm. The H_{σ} values of NFO thin films are 26.2 kOe, 14.1 kOe and 10.9 kOe, for films on (001), (110) and (111) substrates, respectively. The estimated H_{σ} values for bulk single crystal values of λ are much higher than our experiment values of H_u . This discrepancy could be attributed to the large film-substrate lattice mismatch of NFO films and STO substrate. The anticipated substrate clamping effect could therefore result in a reduction in λ compared to the bulk values.^{30,31} Also, the strain relaxation and microstructure defects in NFO films could cause the decrease of H_u .

To understand the residual strain effect on the anisotropic magnetic properties, the strain states of the NFO films have been analysis based on the XRD data. The strain states induced by different oriented substrates can be calculated using the following formula³²:

$$\varepsilon_{zz} = \frac{d_{film} - d_{bulk}}{d_{bulk}} \tag{3}$$

where d_{film} and d_{bulk} are the interplanar distances of the thin film and bulk NFO, respectively. Based on the RSM data, we calculated the out-of-plane lattice parameters of the three oriented NFO films and the corresponding out-of-plane strain (ε_{zz}), respectively, as shown in Table 2. The in-plane strain can be calculated based on the following formula^{32, 33}:

$$\varepsilon_{zz} = -2\nu \varepsilon_{xx} / (1 - \nu) \tag{4}$$

 ε_{zz} is the out-of-plane strain; ε_{xx} is the in-plane strain; ν is Poisson's ratio (estimated for films to be $0.369)^{14}$, assuming an approximate volume preserving distortion. According to Eq. (4), the in-plane strain ε_{xx} for the three oriented thin films is also shown in Table 2. Even though the lattice mismatch between bulk NFO and the substrate is approximately 6.7%, the thin films are partially relaxed. Furthermore, the strain also has a significant influence on the strength of the magnetic anisotropy, which can be attributed to the unquenched orbital momentum of the B-sublattice Ni²⁺ ground state in the inverse spinel material.^{34, 35}

Finally, we compare the growth induced anisotropy field H_u in NFO films on STO to reported values for NFO films deposited by PLD techniques on spinel substrates such as MgAl₂O₄, MgGa₂O₄, and CoGa₂O₄ with a film-lattice mismatch of 3.1%, 0.8% and 0.2%, respectively¹⁷. The anisotropy field attributed to a compressive strain in the film due to substrate-film lattice mismatch for these systems had in-plane anisotropy field with H_u of 0.5 to 11.9 kOe¹⁷. Similarly, very thin PLD films of NiZnAl-ferrite on MgAl₂O₄ were found to have a strain induced easy-plane magnetoelastic anisotropy H_u of 10 kOe¹⁶. In another recent study on epitaxial NiZn-ferrite films with thickness of 2-30 μ m were grown by liquid phase epitaxy on (100) and (111) MgO substrates³⁶. The films were characterized in terms of magnetic order parameters and were found to have growth induced in-plane anisotropy filed that was larger in films on (100) MgO than for films on (111) MgO. **The NFO films fabricated on MgAl₂O₄ (100) with thickness of 47 nm have the similar S-shape**

magnetization behavior as our work, but the film doesn't show FMR signal while the MgFe₂O₄ film with Mg²⁺ replaced Ni²⁺ has an in-plane uniaxial anisotropy of 2.15 kOe.¹² In our work, all three strained NFO films on STO show growth induced out-of-plane uniaxial anisotropy field, in the range of 1.4 ~ 6.1 kOe. The various magnetic strain anisotropy of NFO films on CoGa₂O₄ (001) and (110), can strongly impact the magnetic field induced spin seebeck voltage.¹⁰ And the NFO film grown on MgGa₂O₄ (001) shows the temperature dependence out-of-plane uniaxial magnetic anisotropy field, and the tuning of spin Hall magnetoresistance effect due to the interface quality.¹¹ The key finding in our study is one could control the growth induced anisotropy with proper choice of crystallographic orientation for the substrate and is of importance for potential use of NFO films in spintronic devices.

4. Conclusions

In summary, epitaxial NFO thin films fabricated on (001)-, (110)- and (111)-oriented STO substrates have various strain states due to a large lattice mismatch of 6.7%. Magnetic and FMR measurements were carried out to determine the magnetization and growth induced out-of-plane uniaxial anisotropy field. The NFO film on STO (111) with highest strain shows the smallest perpendicular uniaxial anisotropy field, and the value of the perpendicular uniaxial anisotropy increases with the decrease of strain. The strain control of uniaxial anisotropy significantly impacts the further investment of spin seebeck and spin magnetoresistance effect in NFO thin films, also provide a new way to study the performance of strain engineering on magnetic anisotropy for ferromagnetic thin films.

Acknowledgments

This work was financially supported by the National Natural Science Foundation of China (51372074, 11574073, and 11974104), and Hubei Key Laboratory of Ferro

& Piezoelectric Materials and Devices (201706). The authors would like to thank Mr. Jingyi Chen of PANalytical Division, Spectris Instrumentation & Systems, Shanghai Ltd. for the assistance with RSM measurements. AA thanks NIH NCI (Grant R01CA045424), Research Excellence Fund (REF), and Center for Biomedical Research at Oakland University for support. This material is also based upon work supported by the National Science Foundation under Grant No. CHE-1920110.

References

- ¹U. Lüders, A. Barthélémy, M. Bibes, K. Bouzehouane, S. Fusil, E. Jacquet, J. Contour, J. Bobo, J. Fontcuberta, A. Fert, Adv. Mater. 18, 1733 (2006).
- ²C. N. Chinnasamy, S. D. Yoon, A. Yang, A. Baraskar, C. Vittoria, V. G. Harris, J. Appl. Phys. 101, 09M517 (2007).
- ³Y. Suzuki, R. B. van Dover, E. M. Gyorgy, Julia M. Phillips, V. Korenivski, D. J. Werder, C. H. Chen, R. J. Cava, J. J. Krajewski, W. F. Peck Jr, K. B. Do, Appl. Phys. Lett. 68, 714 (1996).
- ⁴Y. K. Fetisov, A. Bush, K. E. Kamentsev, A. Y. Ostashchenko, G. Srinivasan, IEEE Sensors Journal, 6, 4 (2006).
- ⁵R. K. Kotnala, J. Shah, Handbook of Magnetic Materials, 23, 291 (2015).
- ⁶M. Foerster, J. M. Rebled, S. Estradé, S. Florencio, P. Francesca, J. Fontcuberta, Phys. Rev. B. 84, 144422 (2011).
- ⁷R. C. Budhani, S. Emori, Z. Galazka, B. A. Gray, M. Schmitt, J. J. Wisser, H. M. Jeon, H. Smith, P. Shah, M. R. Page, M. E. McConney, Y. Suzuki, B. M. Howe, Appl. Phys. Lett. 113, 082404 (2018).
- ⁸T. Tainosho, J. Inoue1, S. Sharmin1, M. Takeguchi, E. Kita1, H. Yanagihara, Appl. Phys. Lett. 114, 092408 (2019).
- ⁹R. Adel, Y. S. Chenl, C. H. Huang, J. G. Lin, J. Appl. Phys. 127, 113904 (2020).
- ¹⁰Z. Li, J. Krieft, A. V. Singh, S. Regmi, A. Rastogi, A. Srivastava, Z. Galazka, T. Mewes, A. Gupta, T. Kuschel, Appl. Phys. Lett. 114, 232404 (2019).
- ¹¹M. Althammer, A. V. Singh, T. Wimmer, Z. Galazka, H. Huebl, M. Opel, R. Gross, A. Gupta, Appl. Phys. Lett. 115, 092403 (2019).
- ¹²A. Rastogi, Z. Li, A. V. Singh, S. Regmi, T. Peters, P. Bougiatioti, D. Carsten né Meier, J. B. Mohammadi, B. Khodadadi, T. Mewes, R. Mishra, J. Gazquez, A. Y. Borisevich, Z. Galazka, R. Uecker, G. Reiss, T. Kuschel, A. Gupta, Phys. Rev. Appl. 14, 014014 (2020).
- ¹³T. Dhakal, D. Mukherjee, R. Hyde, P. Mukherjee, M. H. Phan, H. Srikanth, S. Witanachchi, J. Appl. Phys. 107, 053914(2010).

- ¹⁴D. Fritsch, C. Ederer, Phys. Rev. B. 82, 104117 (2010).
- ¹⁵J. A. Heuver, A. Scaramucci, Y. Blickenstorfer, S. Matzen, N. A. Spaldin, C. Ederer, B. Noheda, Phys. Rev. B. 92, 214429 (2015).
- ¹⁶S. Emori, B.A. Gray, H.M. Jeon, J. Peoples, M. Schmitt, K. Mahalingam, M. Hill, M.E. McConney, M.T. Gray, U.S. Alaan, A.C. Bornstein et al, Adv. Mater. 29, 1701130 (2017).
- ¹⁷A.V. Singh, B. Khodadadi, J.B. Mohammadi, S. Keshavarz, T. Mewes, D.S. Negi, R. Datta, Z. Galazka, R. Uecker, A. Gupta, Adv. Mater. 29, 1701222 (2017).
- ¹⁸F. Rigato, S. Estradé, J. Arbiol, F. Peiró, U. Lüders, X. Martí, F. Sánchez, J. Fontcuberta, Mater. Sci. Eng. B.144, 43-48 (2007).
- ¹⁹R. Datta, S. Kanuri, S. V. Karthik, D. Mazumdar, J. X. Ma, A. Gupta, Appl. Phys. Lett. 97, 071907 (2010).
- ²⁰P. Zhou, Y. Qi, C. Yang, Z. Mei, A. Ye, K. Liang, Z. Ma, Z. Xia, T. Zhang, AIP Advances, 6, 125044(2016).
- ²¹C. Chen, A. Saiki, N. Wakiya, K. Shinozaki, N. Mizutani. J. Cryst. Growth. 219, 3 (2000).
- ²²D. Roy, S. Sakshath, G. Singh, R. Joshi, S. V. Bhat, P. S. Anil Kumar. J. Phys. D: Appl. Phys. 48, 12 (2015).
- ²³ Y. Suzuki, Annu. Rev. Mater. Res. 31, 265-289 (2001).
- ²⁴S. Venzke, R. B. Van Dover, J. M. Phillips, E. M. Gyorgy, T. Siegrist, C. H. Chen, D. Werder, R. M. Fleming, R. J. Felder, E. Coleman, R. Opila, J. Mater. Res. 11, 1187-1198 (1996).
- ²⁵P. Zhou, A. V. Singh, Z. Li, M. A. Popov, Y. Liu, D. A. Filippov, T. Zhang, W. Zhang, P. J. Shah, B.M. Howe, M.E. McConney, G. Srinivasan, M. R. Page, A. Gupta, Phys. Rev. Appl. 11, 054045 (2019).
- ²⁶R. Naik, C. Kota, J. S. Payson, G. L. Dunifer, Phys. Rev. B 48, 1008 (1993).
- ²⁷J. Smith, H. G. Beljers, Phillips Res. Rep. 10, 113-130 (1955).
- ²⁸Landolt-Bornstein; Numerical data and functional relationships in science and technology, Group III, Crystal and Solid State Physics, vol 4(b), Magnetic and Other Properties of Oxides, eds. K.-H. Hellwege and A. M. Springer, Springer-Verlag, New

York (1970).

²⁹Y. Suzuki, G. Hu, R. B. Van Dover, R. J. Cava, J. Magn. Magn. Mater. 191, 1-8 (1999).

³⁰R. Varghese, R. Viswan, K. Joshi, S. Seifikar, Y. Zhou, J. Schwartz, S. Priya, J. Magn. Magn. Mater. 363, 179-187 (2014).

³¹C. W. Nan, G. Liu, Y. Lin, H. Chen. Phys. Rev. Lett. 94, 19 (2005).

³²C. Adamo, X. Ke, H. Q. Wang, H. L. Xin, T. Heeg, M. E. Hawley, W. Zander, J. Schubert, P. Schiffer, D. A. Muller, L. Maritato, D. G. Schlom, Appl. Phys. Lett. 95, 112504 (2009).

³³S. Z. Wu, J. Miao, X. G. Xu, W. Yan, R. Reeve, X. H. Zhang, Y. Jiang, Sci. Rep. 5, 8905 (2015).

³⁴J. Chen, G. Srinivasan, S. Hunter, V. Suresh Babu, M. S. Seehra, J. Magn. Magn. Mater. 146, 291-297 (1995).

³⁵Seifikar, A. Tabei, E. Sachet, T. Rawdanowicz, N. Bassiri-Gharb, J. Schwartz, J. Appl. Phys. 112, 063908 (2012).

³⁶P. Zhou, M. A. Popov, Y. Liu, R. Bidthanapally, D. A. Filippov, T. Zhang, Y. Qi, P.J. Shah, B.M. Howe, M.E. McConney, Y. Luo, G. Sreenivasulu, G. Srinivasan, M. R. Page, Phys. Rev. Mater. 3, 044403 (2019).

Figure captions

- Figure 1. θ -2 θ scans of NFO thin films by X-ray diffraction with different orientations, where the top panel, middle panel, and bottom panel denote (111)-oriented, (110)-oriented, and (001)-oriented samples, respectively.
- Figure 2. X-ray diffraction RSMs around STO (002) and NFO (004) crystallographic planes, STO (220) and NFO (440) crystallographic planes, and STO (222) and NFO (444) crystallographic planes, for (001)-, (110)-, and (111)-oriented samples, respectively.
- Figure 3. TEM images of NFO thin films grown on (001)-, (110)-, and (111)-oriented STO substrates. (a) Cross-sectional TEM image of NFO/STO, SAED patterns obtained from (b) film-substrate interface and (c) NFO film, (d) HRTEM image from the film-substrate interface.
- Figure 4. The curves M/M_s versus H of (a) (001)-, (b) (110)-, and (c) (111)-oriented NFO thin films. The corresponding insets show the M-H on expanded field axes.
- Figure 5. In-plane and out-of-plane FMR spectrum at 9.3 GHz for (a) (001)-, (b) (110)-, and (c) (111)-oriented NFO thin films on STO. Inset in (a) shows the magnetic field configuration.
- Figure 6. The magnetostriction versus H for (001), (110), and (111) orientations of NFO single crystal.
- Table 1. The gyromagnetic ratio $\gamma = 3$ GHz/kOe, the in-plane orientation ψ_M and out-of-plane orientation θ of magnetization vector \mathbf{M} , the effective magnetization $4\pi M_{\rm eff}$, saturation magnetic field $4\pi M_{\rm s}$, cubic magnetocrystalline anisotropic field H_4 , growth induced uniaxial anisotropy field H_u and estimated strain anisotropy H_{σ} of NFO film with different orientation can be obtained from M-H and FMR according to equation (1) and (2).
- Table 2. The lattice parameter of NFO film with different orientation can be calculated from the RSM in Fig. 2. The out-of-plane and in-plane strain of three oriented NFO film are calculated according to equation (3) and (4).

Figure 1

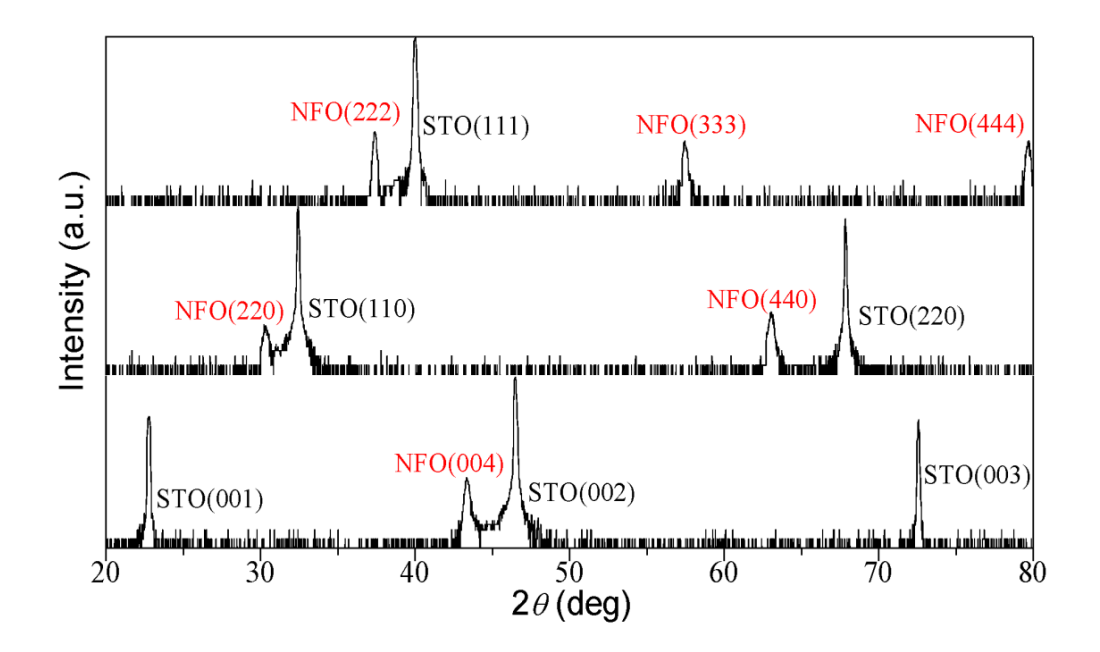


Figure 2

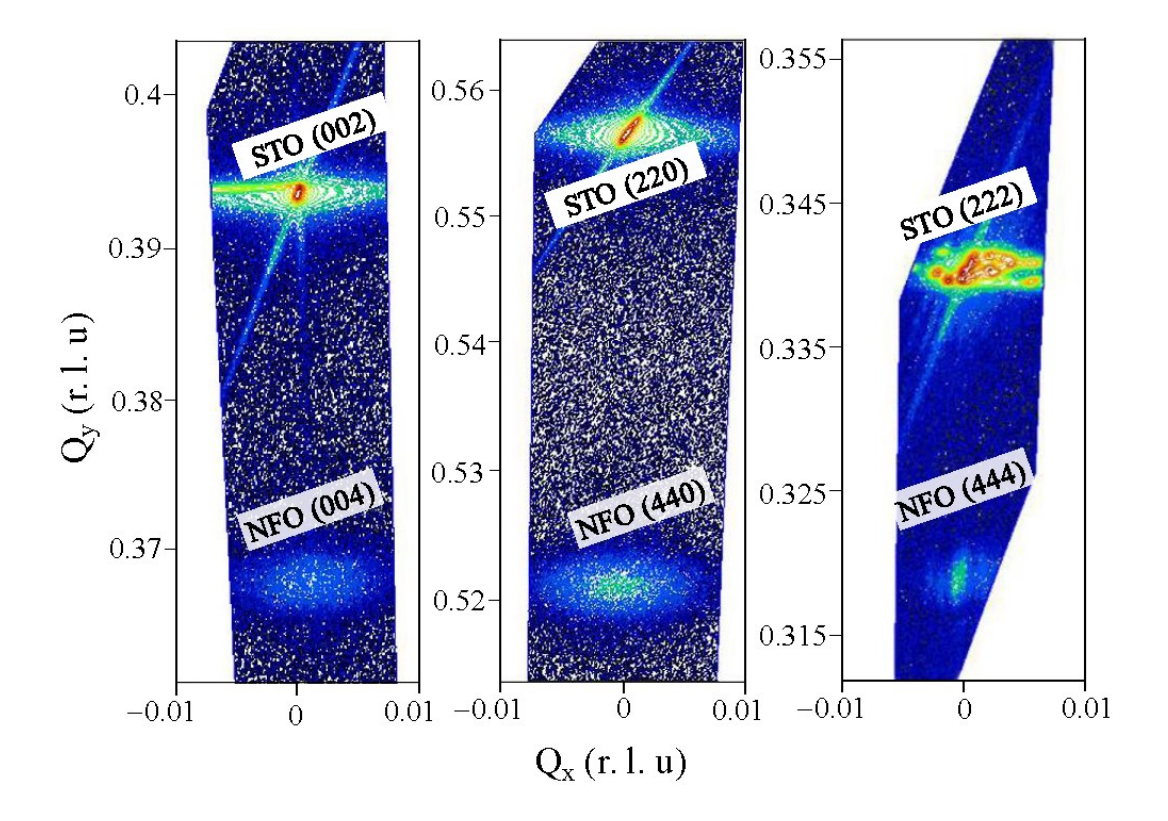


Figure 3

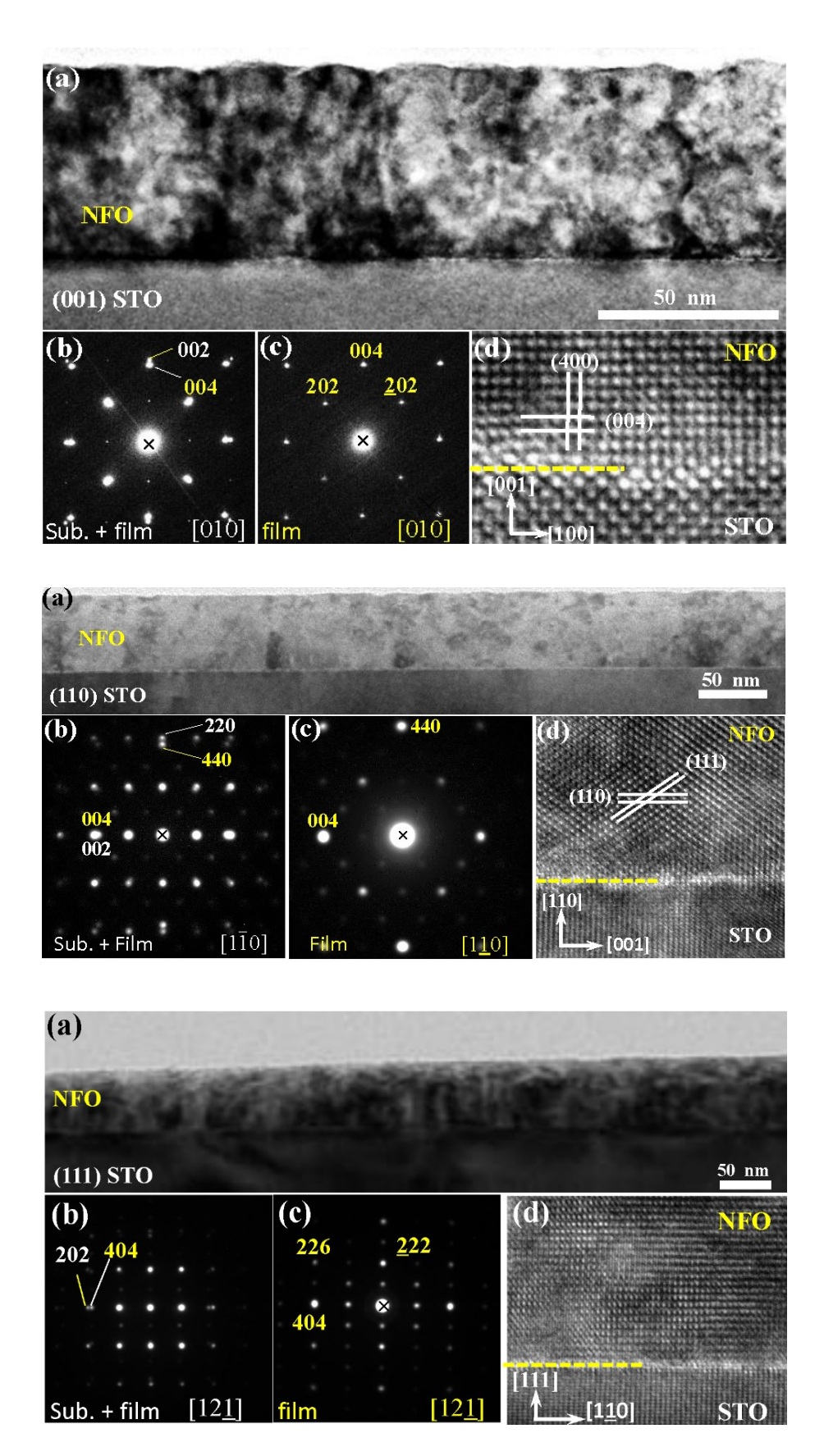


Figure 4

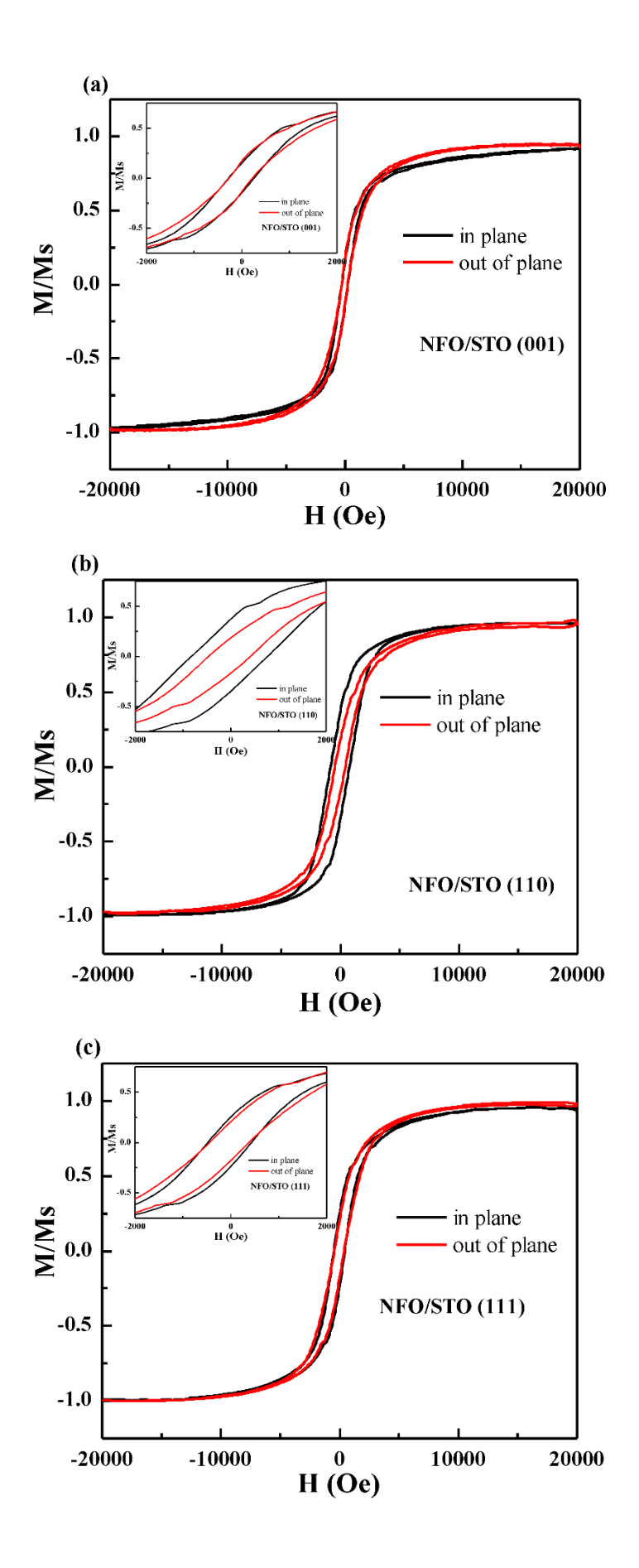


Figure 5

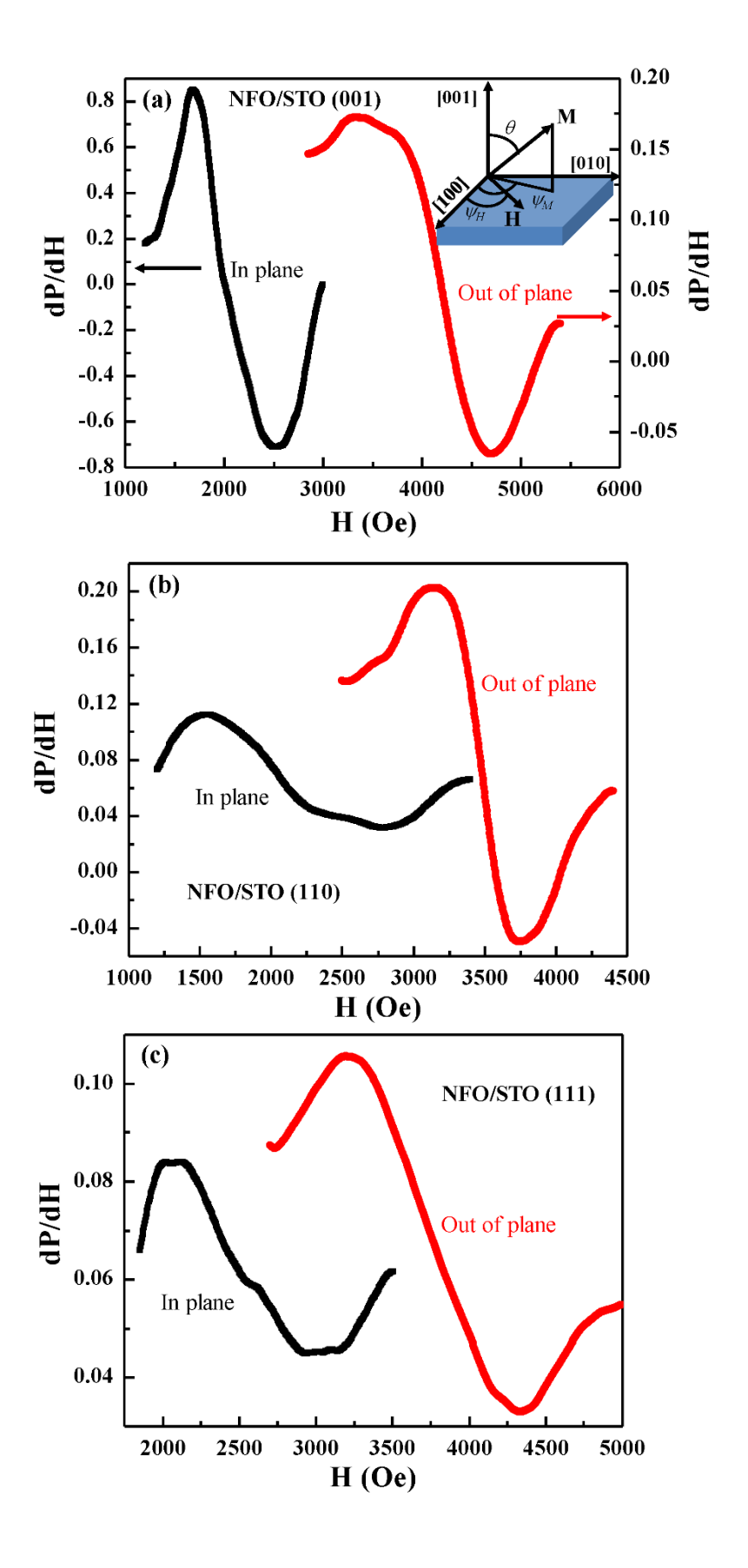


Figure 6

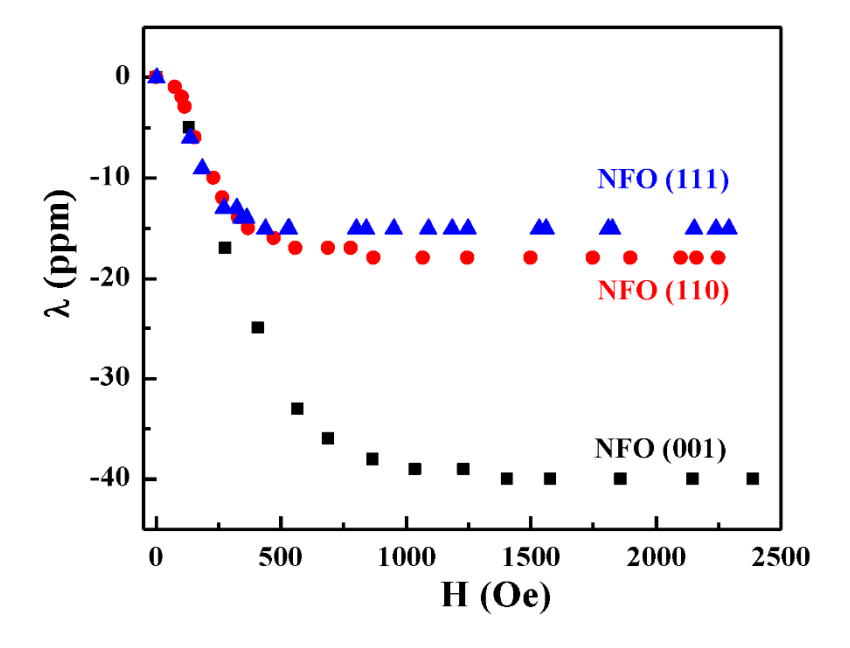


Table 1.

Structure	Ψм	θ	4πM _{eff} (kOe)	4πM _s (kOe)	H ₄ (kOe)	H _u (kOe)	H _σ (kOe)
NFO/STO (001)	63°	-19°	-3.101	3.027	-0.5	6.128	26.2
NFO/STO (110)	63°	-23°	-3.311	2.512	-0.5	5.823	14.1
NFO/STO (111)	-11°	0°	-1.564	3.027	-0.5	1.463	10.9

Table 2.

Structure	Film	d bulk (Å)	dfilm (Å)	$\boldsymbol{arepsilon}_{\mathbf{z}\mathbf{z}}$	$\boldsymbol{\varepsilon}_{xx}$
NFO/STO (001)	NFO (004)	8.339	8.472	1.59%	-1.36%
NFO/STO (110)	NFO (440)	5.897	5.804	-1.58%	1.35%
NFO/STO (111)	NFO (444)	4.815	4.729	-1.78%	1.52%